

Raman-Based Silicon Photonics

Bahram Jalali, *Fellow, IEEE*, Varun Raghunathan, *Student Member, IEEE*, Dimitri Dimitropoulos, and Özdal Boyraz, *Member, IEEE*

(Invited Paper)

Abstract—This paper reviews recent progress in a new branch of silicon photonics that exploits Raman scattering as a practical and elegant approach for realizing active photonic devices in pure silicon. The large Raman gain in the material, enhanced by the tight optical confinement in Si/SiO₂ heterostructures, has enabled the demonstration of the first optical amplifiers and lasers in silicon. Wavelength conversion, between the technologically important wavelength bands of 1300 and 1500 nm, has also been demonstrated through Raman four wave mixing. Since carrier generation through two photon absorption is omnipresent in semiconductors, carrier lifetime is the single most important parameter affecting the performance of silicon Raman devices. A desired reduction in lifetime is attained by reducing the lateral dimensions of the optical waveguide, and by actively removing the carriers with a reverse biased diode. An integrated diode also offers the ability to electrically modulate the optical gain, a unique property not available in fiber Raman devices. Germanium-silicon alloys and superlattices offer the possibility of engineering the otherwise rigid spectrum of Raman in silicon.

Index Terms—Nonlinear optics, Raman amplification, Raman laser, silicon, wavelength conversion.

I. INTRODUCTION

THE recent wide-scale interest in silicon photonics can be identified with two motives. First, being able to tap into silicon's vast manufacturing base will reduce the cost of photonic devices which, in turn, will accelerate penetration of optics into communication at shorter distances than today's fiber optic networks. Additionally, the technology can solve important problems in today's computing systems, as well as spawn new industries of its own. For example, as the trend to reducing device dimensions continues, a significant bottleneck has appeared at the electronics interconnect level, where a large gap exists between individual device speeds and the speed of interconnects that link them [1], [2]. Optical interconnects can potentially solve this important problem.

In the 1990s, a large number of passive silicon devices were developed [3] with a few reaching commercialization. However, due to unfavorable physical properties, such as the lack of efficient optical transitions due to the indirect band structure and the near-absence of Pockel's effect caused by symmetric crystal structure, creation of active devices proved to be much more difficult.

Manuscript received August 26, 2005.

B. Jalali, V. Raghunathan, and D. Dimitropoulos are with the Department of Electrical Engineering, University of California, Los Angeles, CA 90095-1594 USA (e-mail: jalali@ucla.edu; varun@ee.ucla.edu; ddmtr@ee.ucla.edu).

Ö. Boyraz is with the Department of Electrical Engineering and Computer Science, University of California, Irvine, CA 92697-2625 USA (e-mail: oboyraz@uci.edu).

Digital Object Identifier 10.1109/JSTQE.2006.872708

The prospects for active optical functionality in silicon have drastically improved since the adoption of the Raman effect as a mechanism for producing amplifiers, lasers, and wavelength converters. Last year was witness to the demonstration of the first silicon laser [4]. The rapid pace of progress is continuing, and the first quarter of 2005 has already seen the demonstration of direct electrical modulation of the Raman laser [5] and report of the first continuous-wave (CW) silicon Raman laser [6].

Raman scattering was proposed and demonstrated in 2002 as a mean to bypass these limitations, and to create optical amplifiers and lasers in silicon [7]. The approach was motivated by the fact that the stimulated Raman gain coefficient in silicon is 10^3 – 10^4 times larger than that in fiber. The modal area in a silicon waveguide is roughly 100 times smaller than in fiber, resulting in a proportional increase in optical intensity. The combination makes it possible to realize chip-scale Raman devices that normally require kilometers of fiber to operate. The initial demonstration of spontaneous Raman emission from silicon waveguides in 2002 was followed by the demonstration of stimulated Raman scattering [8] and parametric Raman wavelength conversion [9], both in 2003. Other merits of the Raman effect include the fact that it occurs in pure silicon and hence does not require rare earth dopants (such as Erbium), and that the spectrum is widely tunable through the pump laser wavelength.

II. RAMAN SCATTERING IN SILICON

Classical electrodynamics provides a simple and intuitive macroscopic description of the Raman scattering process [10]. In the spontaneous scattering, thermal vibrations of a lattice at frequency ω_v (15.6 THz in silicon) produce a sinusoidal modulation of the susceptibility. The incident pump field induces an electric polarization that is given by the product of the susceptibility and the incident field. The beating of the incident field oscillation ω_p with oscillation of the susceptibility ω_v produces induced polarizations at the sum frequency $\omega_p + \omega_v$, and at the difference frequency $\omega_p - \omega_v$. The radiation produced by these two polarization components is referred to as anti-Stokes and Stokes waves, respectively. Quantum statistics dictates that the ratio of Stokes power to anti-Stokes power is given by $(1 + N)/N$, where $N = [\exp(\hbar\omega_v/kT) - 1]^{-1}$ is the Bose occupancy factor, and has a value of ~ 0.1 for silicon at room temperature.

The same model can be extended to describe stimulated Raman scattering [10]. Here, one assumes that pump and Stokes fields are present, with a frequency difference equal to the atomic vibrational frequency. The latter can be due to spontaneous emission, or in the case of a Raman amplifier,

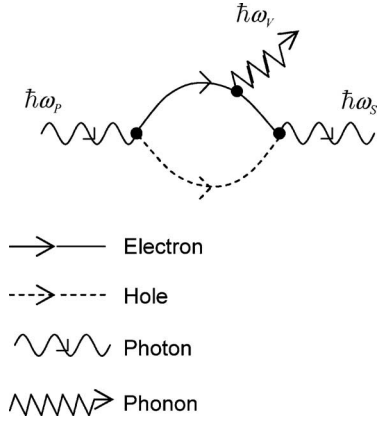


Fig. 1. Feynman diagram for Stokes Raman scattering process characterized by emission of a phonon. Diagram for anti-Stokes scattering is the same, but with the phonon being absorbed rather than emitted.

it is the input signal that is to be amplified. The two fields (pump and Stokes) create a force that stimulates atomic vibrations, even in the absence of a dipole moment. This can be understood as follows. If E is the total field comprising of pump and Stokes and χ is the susceptibility, the energy stored in the field, $V = ((1 + \chi)/2)E \cdot E^*$, will have a component oscillating at $\omega_p - \omega_s = \omega_v$. Through the modulation of the susceptibility with displacement Q , this will produce a force $F \propto (\partial V / \partial Q) \approx (\partial \chi / \partial Q) E_p \cdot E_s \cdot \exp(-i\omega_v \cdot t)$. This driving force will enhance atomic oscillations which, in turn, will increase the amplitude of the Stokes field E_s . This positive feedback phenomenon is called stimulated Raman scattering and results in the amplification of the Stokes field.

While providing an intuitively appealing description of Raman scattering, the macroscopic model previously described does not account for detailed processes responsible for Raman scattering in silicon. The microscopic picture reveals that the direct coupling of light with atomic vibrations, described by the interaction Hamiltonian involving photons and phonons, is very weak. This is generally true in semiconductors due to the large atomic mass that appears (squared) in the denominator of the cross section. In silicon, the lack of dipole moment further underscores this fact. Electrons mediate the Raman scattering process in silicon. Microscopically, the scattering proceeds in three steps [11]. In step one, the incident photon excites the semiconductor into an intermediate step by creating an electron-hole pair. In step two, the pair is scattered into another state by emitting a phonon via the electron-phonon interaction Hamiltonian. In step three, the electron-hole pair in the intermediate step recombines radiatively with emission of a scattered photon. While electrons mediate the process, they remain unchanged after the process. Furthermore, transitions involving electrons are virtual, and hence do not need to conserve energy, although momentum must be conserved. The Feynman diagram for the process is shown in Fig. 1.

The Raman scattering process involves the optical phonon branches of atomic vibrations (as opposed to Brillouin, which describes scattering involving acoustic phonons). In first-order scattering, only one phonon is involved, and momentum con-

servation implies that only zone-center phonons can participate. Higher order Raman scattering involves multiple phonons, which can be from any point in the Brillouin zone as long as their total momentum equals the (negligible) photon momentum, provided that the selection rules allow it. In silicon, the zone center optical phonon is triply degenerate with a frequency of 15.6 THz. The first order resonance, which is of primary importance here, has a full-width at half-maximum (FWHM) of approximately 10 GHz [12]. This imposes a maximum information bandwidth of approximately 10 GHz that can be amplified. The Raman linewidth becomes broader when a broadband pump is used.

Crystal symmetry imposes a selection rule that dictates which scattering geometries are allowed. The spontaneous scattering efficiency S is given by

$$S = S_0 \sum_{k=1,2,3} |\hat{e}_s \cdot R_k \cdot \hat{e}_p|^2.$$

Unit vectors \hat{e}_p and \hat{e}_s denote the polarization of the pump and Stokes electromagnetic fields, respectively. S_0 contains intrinsic microscopic property of silicon including derivatives of the polarizability, and the absolute amplitude of the displacement of the zone-center optical phonons. The sum runs over the three Raman matrices, each corresponding to the phonon displacement along one of the three principle axes of the crystal [13]

$$\vec{R}_1 = \begin{bmatrix} 0 & 0 & 0 \\ 0 & 0 & 1 \\ 0 & 1 & 0 \end{bmatrix} \quad \vec{R}_2 = \begin{bmatrix} 0 & 0 & 1 \\ 0 & 0 & 0 \\ 1 & 0 & 0 \end{bmatrix} \quad \vec{R}_3 = \begin{bmatrix} 0 & 1 & 0 \\ 1 & 0 & 0 \\ 0 & 0 & 0 \end{bmatrix}.$$

In the preceding representation, the correspondence between vectors and crystal directions is $\hat{e}_1 = (1, 0, 0) \equiv [100]$, $\hat{e}_2 = (0, 1, 0) \equiv [010]$ and $\hat{e}_3 = (0, 0, 1) \equiv [001]$. In standard wafer technology, the waveguides are fabricated on a (001) surface and are parallel to the [110] direction. So that in a silicon-on-insular (SOI) rib waveguide that supports a transverse electric (TE) and a transverse magnetic (TM) mode and is fabricated along [110] the polarization directions are $\hat{e}_{TE} = (1/\sqrt{2})(1, -1, 0)$ and $\hat{e}_{TM} = (0, 0, 1)$.

The Raman gain coefficient g_R can be obtained from the spontaneous efficiency S using the Einstein relation, as [14]

$$g_R = \frac{8\pi c^2 \omega_p}{\hbar \omega_s^4 n^2(\omega_s)(N+1)\Delta\omega} S.$$

Substituting the appropriate values, the gain coefficient is obtained as ~ 76 cm/GW [7]. This uses $S = 8.4 \times 10^{-7} \text{ cm}^{-1} \text{ Sr}^{-1}$, which was obtained by extrapolating the values measured 1.1 μm wavelength to 1.55 using a λ^{-4} relation. This is in the same order of magnitude but several times larger than the values extracted from Raman gain measurements (~ 20 cm/GW) at 1.55 μm [8]; nonetheless, when compared to silica (0.93×10^{-2} cm/GW), the Raman gain in silicon is $10^3 - 10^4$ times larger. Such a large difference has its origin in the much narrower linewidth of the Raman spectrum in crystalline silicon, compared to the amorphous fiber.

It is customary to describe the induced polarization for the case of stimulated Raman scattering through the nonlinear susceptibility χ_{ijmn}^R , defined by

$$P_i^{\text{NL}}(\omega_s) = \varepsilon_0 \chi_{ijmn}^R E_j(\omega_p) E_m(-\omega_p) E_n(\omega_s).$$

On the other hand, the atomic displacement can be obtained using a classical harmonic oscillator model [10] with the driving force described previously. By comparing the induced polarization suggested by the displacement with the preceding definition, one arrives at the following expression for the induced Raman susceptibility:

$$\chi_{ijmn}^R = 2\Gamma\omega_V \frac{2ncg_R}{\omega_s(\mu_0/\epsilon_0)^{1/2}} \frac{\sum_{k=1,2,3}(R_{ij})_k(R_{mn})_k}{(\omega_V^2 - (\omega_p - \omega_s)^2 - 2i\Gamma(\omega_p - \omega_s))}$$

Where Γ is the dissipative term in the harmonic oscillator equation, and n is the refractive index. Crystal symmetry consideration, described by the Raman tensor R , leads to a total of 12 equal nonvanishing components that have the indexes of the form

$$\begin{aligned} 1221 &= 1212 = 2112 = 2121 = 1331 = 1313 \\ &= 3113 = 3131 = 2332 = 2323 = 3223 = 3232. \end{aligned}$$

The induced susceptibility is related to the Raman gain coefficient as [13]

$$\begin{aligned} \chi_{1221}^R(\omega_p - \omega_s = \Omega) &= \frac{i}{(\mu_0/\epsilon_0)^{1/2}} \frac{2ncg_R}{\omega_s} \\ &= 11.2 \times 10^{-14} i \frac{\text{cm}^2}{V^2}. \end{aligned}$$

Two-photon-absorption (TPA) is another nonlinear optical effect that is particularly strong in semiconductors. This effect results in pump depletion and generation of free carriers that, through the free carrier plasma effect, gives rise to a broadband absorption spectrum. TPA has been shown to be negligible from the point of view of pump depletion [8]. This is plausible since the TPA coefficient in silicon, β , is relatively small, ~ 0.5 cm/GW. On the other hand, absorption by TPA-generated free carriers is a broadband process that competes with the Raman gain. The effect has been identified as a limiting factor in all-optical switching in III-V semiconductor waveguides [15]–[19]. It has also been discussed as a potential limit to achievable Raman gain in GaP waveguides [20], although a Raman gain of 24 dB was demonstrated in these waveguides [21]. More recently, TPA-induced FCA has been measured in silicon waveguides in the context of the Raman process [22], [23] and in the transmission of ultrashort pulses in silicon waveguides [24].

The magnitude of TPA-induced free carrier absorption depends on free carrier concentration through the relation: $\alpha^{\text{FCA}} = 1.45 \times 10^{-17} (\lambda/1.55)^2 \cdot \Delta N$, where λ is the wavelength in microns, and ΔN is the density of electron-hole pairs [25], [26]. The latter is related to the pump intensity I_p by

$$\Delta N = \beta \cdot I_p^2 \cdot \tau_{\text{eff}} / (2 \cdot h\nu)$$

where $h\nu$ is the pump photon energy and τ_{eff} is the effective recombination lifetime for free carriers. This equation neglects the contribution to free carrier generation due to pump-signal

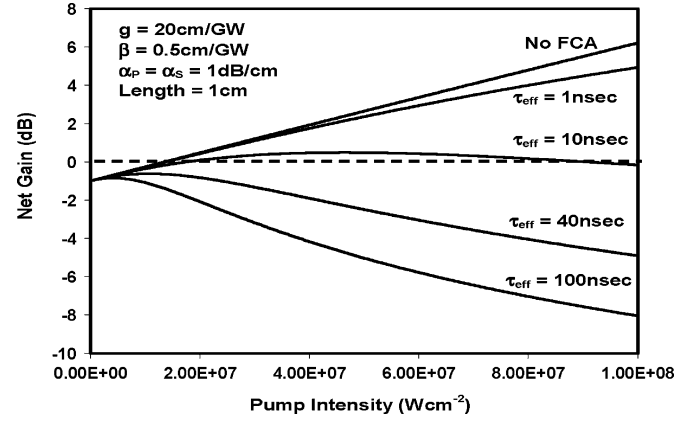


Fig. 2. Impact of carrier lifetime on achievable CW Raman gain. Gain increases with intensity, while loss rises as intensity squared and dominates when lifetime is long.

TPA, and hence is valid in the regime where Stokes intensity $(I_s)I_s \ll I_p$.

The fundamental parameter that governs the TPA induced loss, and hence the success of Raman-based devices, is the recombination lifetime τ_{eff} . It is well known that the recombination lifetime in SOI is much shorter than that in a bulk silicon sample with comparable doping concentration. This lifetime reduction is due to the presence of interface states at the boundary between the top silicon and the buried oxide layer. This effect depends on the method used for preparation of the SOI wafer and the film thickness, with measured and expected values ranging between 10–200 ns [27]–[29]. In SOI waveguides, the lifetime is further reduced to a few nanoseconds, or even below in the case of submicron waveguides, due to the recombination at the etched waveguide facets and, in the case of rib waveguides, to diffusion into the slab regions [29]. The lifetime can be further reduced by application of a reverse-bias p-n junction [22], [23], [29], or by introduction of midgap states through high energy irradiation, and gold or platinum doping. Modest amount of CW gain has been observed in deep submicrometer waveguides [30] where the impact of surface and interface recombination plays a critical role in reducing the lifetime. CW gain has also been demonstrated by sweeping the free carriers using a reverse-bias p-n junction [31]. This approach is further discussed in the context of Raman laser in the following.

The plot of the net Raman gain as a function of CW pump intensity for a waveguide of length $L = 1.9$ cm and propagation loss 1 dB/cm is shown in Fig. 2 [23] for different free carrier lifetime values. The plot shows that more than 5 dB of gain can be obtained with a pump intensity of less than 100 MW/cm². Gain increases with intensity, while the loss rises as intensity squared and dominates when the lifetime is long. The pump is assumed to be a monochromatic source. The finite linewidth of the pump laser will result in a lower gain than that predicted in Fig. 2. It is clear that to create a successful amplifier, an effective lifetime of ≤ 1 ns is required.

From the plot in Fig. 2, it is clear that the carrier lifetime is a critical parameter in the operation of a Raman amplifier. In a rib SOI waveguide, its value is determined by the combination

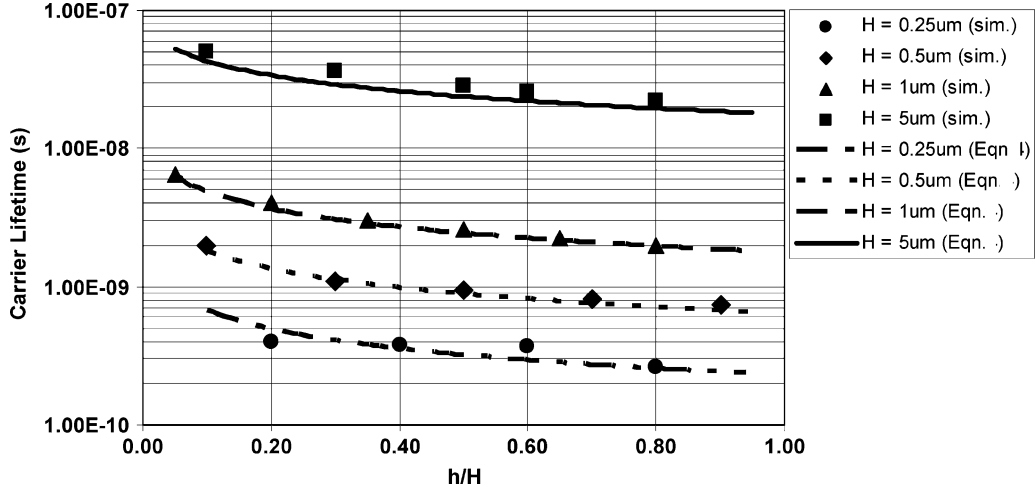


Fig. 3. Dependence of carrier lifetime on ratio h/H for waveguides with $w = H = 0.25, 0.5, 1, \text{ and } 5 \mu\text{m}$ (after [29]).

of carrier diffusion and carrier recombination in the bulk, on the Si surface, and the Si–SiO₂ interface. An analytical expression describing this process is [29]

$$\frac{1}{\tau_{\text{eff}}} = \frac{1}{\tau_b} + \frac{S}{H} + \frac{w + 2(H - h)}{wH} S' + 2 \frac{h}{H} \sqrt{\frac{D}{w^2} \left(\frac{1}{\tau_b} + \frac{S + S'}{h} \right)}.$$

In this expression, τ_b is the carrier recombination lifetime in bulk silicon, S and S' are the interface and surface recombination velocities, D is the ambipolar diffusion coefficient, w is the waveguide rib width, h equals the slab height, and H is the total rib height. The first term in the equation is the contribution of the bulk recombination, the second the contribution of interface recombination, the third the contribution of surface recombination, and the last term is due to the diffusion of carriers out of the rib (and subsequent recombination outside of the waveguide rib). Because τ_b is on the order of 1–100 μs and the surface recombination is often negligible (for passivated good quality silicon surfaces), the lifetime is often determined by the interface recombination. This is especially true for submicron waveguides, because the distance of the generated electrons from the interface where they can recombine is small, and therefore the electron recombination more effective.

As an example, we show in Fig. 3 the dependence of the carrier lifetime on waveguide dimensions [29]. The analytical expression and simulation results for the carrier lifetime are shown for waveguides with $w = H$, where $H = 0.25, 0.5, 1, \text{ and } 5 \mu\text{m}$, where the ratio h/H is varied. The interface recombination velocity is taken to be 8000 cm/s and the surface recombination is neglected. By varying the waveguide dimensions, variation in the carrier lifetime of about two orders of magnitude can be achieved in this example.

Besides engineering the waveguide dimensions to reduce the lifetime, the generated carriers can be swept out of the waveguide core by means of a p-n junction that can be formed by doping regions adjacent to the waveguide core [6]. The use of p-n junction for carrier sweep-out in the silicon waveguide is

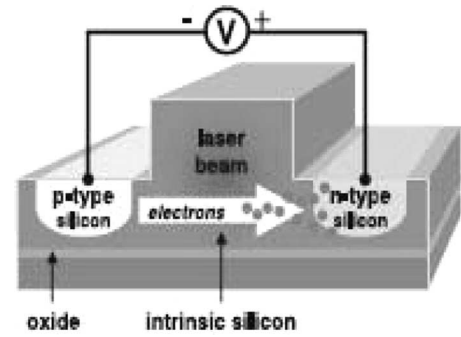


Fig. 4. Carrier sweep-out using p-n junction (from [6]).

shown in Fig. 4. In the case of a strong reverse bias field, the carrier lifetime is determined by the drift current that is due to the applied electric field. The carrier lifetime is the mean transit time of the carriers out of the rib, and equals $\tau_e = w/(2v_e)$ for electrons and $\tau_h = w/(2v_h)$ for holes, where v_e, v_h are the electron and hole velocities, respectively. The velocities, in turn, are a nonlinear function of the applied electric field (the proportionality constant is the carrier mobility), but at very high electric fields, the carrier velocities are independent of the field. The preceding expression gives an estimate for the carrier lifetime in the case where the generation of electron-hole pairs is low. At very high generation rates, the junction might become ineffective because, as the electrons and holes drift in opposite directions, an opposing electric field is build up that is opposing the applied reverse field. In very extreme cases, the junction can be rendered completely ineffective so that the applied field has practically no effect on the lifetime, and the lifetime then is the same as the lifetime in a bare waveguide.

III. RAMAN WAVELENGTH CONVERSION

The nature of the Raman scattering process occurring in the medium is determined by the phase mismatch between the pump, Stokes, and anti-Stokes fields. The total phase mismatch

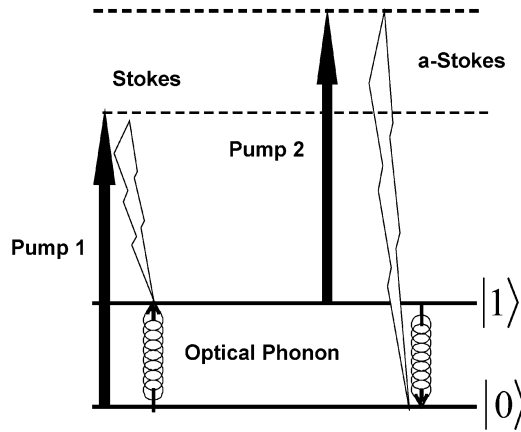


Fig. 5. Energy-level representation of Raman wavelength conversion process. $|1\rangle$ and $|0\rangle$ are vibrational states, and arrow represent virtual transitions. A phonon is created and annihilated, leaving the phonon population unchanged.

is defined as

$$\Delta\beta = 2\beta_p - \beta_s - \beta_{aS}$$

where β is the wave-vector for the given wavelength, and the corresponding mode of polarization should be taken into account.

When the phase mismatch is larger, a stimulated Raman scattering process dominates. This was described in Section II. In this case, the gain coefficient for the anti-Stokes wave will have a negative sign, indicating that an incident anti-Stokes wave will be attenuated. When the phase mismatch is small (close to zero), the anti-Stokes signal can be generated through four-wave mixing (FWM) induced through the Raman susceptibility, in much the same way that conventional FWM takes place via the electronic 3rd order nonlinear susceptibility (responsible for the Kerr effect). In the Raman process, the energy conservation dictates that $\omega_{aS} = 2\omega_p - \omega_s$, and momentum conservation is satisfied by phase matching. In this process, pump, Stokes, and anti-Stokes waves experience coherent interaction. This phenomenon is referred to as coherent anti-Stokes Raman scattering (CARS) in the spectroscopy literature, and was first observed in silicon in 2003 [9]. A similar process can also occur from anti-Stokes to Stokes fields. As shown in Fig. 5, the process of the creation of the anti-Stokes photon is accompanied by creation and annihilation of a zone center phonon. This process can be used to perform wavelength conversion from the Stokes to the anti-Stokes bands. A typical application of this scheme when pumped at 1400 nm is as a chip-scale interface between the technologically important telecom bands; namely, the 1300- and 1550-nm bands. This process is schematically depicted in Fig. 6.

The conversion efficiency is highly sensitive to the phase mismatch and, in general, the efficiency has a sinc^2 dependence on phase mismatch. In silicon, phase mismatch is dominated by the material dispersion, as waveguide dispersion is relatively negligible unless it occurs in waveguides with submicron modal dimensions. In such devices, waveguide dispersion provides a means to compensate for material dispersion. Other means

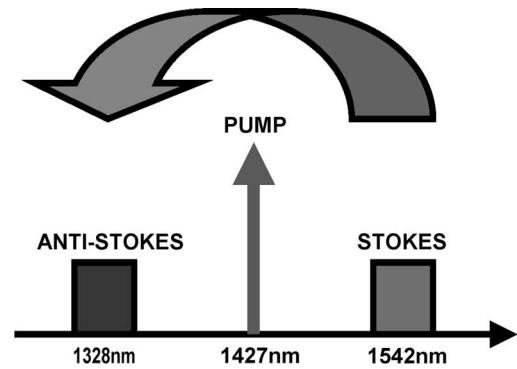


Fig. 6. CARS wavelength process as a chip-scale interface between the 1300 and 1550-nm telecom bands. The waveguide is pumped around 1427-nm.

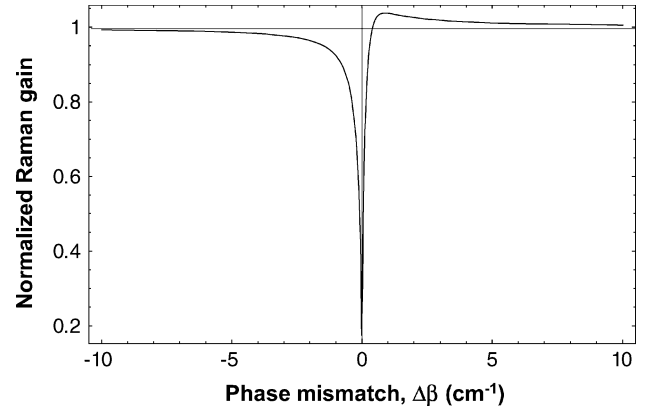


Fig. 7. Variation of normalized Raman gain as a function of phase mismatch. At zero phase mismatch, Raman gain is suppressed in favor of parametric Stokes to anti-Stokes conversion.

of phase matching include the use of waveguide birefringence, which is determined by the waveguide dimensions and the built-in stress. At phase matching, the evolution of Stokes and anti-Stokes fields $E(z)$ along the waveguide length z is given by

$$E_S(z) = E_S(0) + (E_S(0) + E_{aS}^*(0))g_R I_P z/2,$$

$$E_{aS}^*(z) = E_{aS}^*(0) - (E_S(0) + E_{aS}^*(0))g_R I_P z/2.$$

The preceding equation predicts a linear increase in the fields with distance which holds true for small propagation lengths. Once the Stokes and anti-Stokes fields become equal in amplitude, no further change takes place, leading to a saturation effect. The characteristic length is very long; therefore, this regime is not expected to occur in chip-scale devices.

Fig. 7 shows the normalized Raman gain as a function of phase mismatch. At large values of $|\Delta\beta|$, stimulated Raman amplification is the predominant effect and leads to the amplification of the Stokes signal with an effective gain given by g_R . Under phase matching conditions, Raman gain is suppressed and the parametric coupling of pump and Stokes to anti-Stokes dominates. In this region, Stokes, anti-Stokes, and pump fields are strongly coupled and parametric conversion dominates. For small positive values of $\Delta\beta$, the normalized gain slightly exceeds unity due to modulation instability. This effect has also been predicted and observed in optical fibers [32].

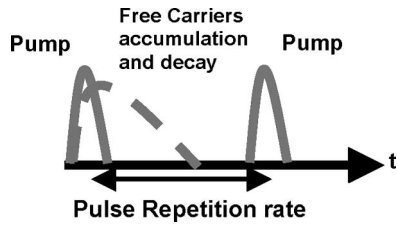


Fig. 8. schematic showing pulsed pumping scheme. Repletion rate of laser is made longer than the carrier lifetime to prevent free-carrier accumulation. Pulswidth of laser is also made longer than phonon response time.

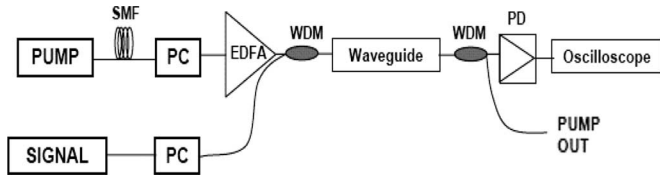


Fig. 9. Experimental setup used to demonstrate pulse-pumped Raman amplifier.

IV. EXPERIMENTAL DEMONSTRATION OF RAMAN DEVICES IN SILICON

Two schemes have been successfully employed to mitigate the deleterious effects of free-carrier losses. One method for avoiding free carrier accumulation and the concomitant loss is pulsed pumping [34]–[37]. As long as the pump pulse period is longer than the free carrier lifetime, the free carrier accumulation can be mostly eliminated. Fig. 8-shows a time-domain schematic of the pulsed pumping scheme. The decay of free-carriers at the trailing edge of the pump pulse ensures that free-carriers do not accumulate, and hence do not contribute to excess nonlinear losses. It should be noted that the pump pulswidth is required to be longer than the phonon response time to ensure that sufficient gain is achieved in the medium. This scheme was employed at UCLA to demonstrate the first silicon Raman laser [4]. Another method to deal with free carriers is to employ reverse-biased carrier sweepout. This scheme was described in the context of lifetime reduction in the waveguides in Section II. Intel has employed this scheme to demonstrate a CW Raman laser [8].

Fig. 9 shows the schematic of the experimental setup used to observe pulsed Raman amplification. The pump and Stokes signal lasers with appropriate polarizations are combined into the waveguide using WDMs. The measured change in CW signal beam (tuned to the peak of Stokes resonance) due to the pump pulse is shown in Fig. 10. The pump source was a mode-locked fiber laser with 25-MHz repetition rate and ~ 1 -ps output pulse width. Since phonon response time in silicon is more than 3 ps, the pulse width is broadened by using a spool of standard single mode optical fiber. Maximum pump on-off gain of 20 dB has been obtained. Taking into account the losses in the waveguide, we obtain a net waveguide gain of 13 dB [37]. This gain includes waveguide propagation losses, but not the fiber-waveguide coupling loss. In separate devices that have adiabatic mode tapers, we have shown a net fiber-to-fiber gain of 11 dB under a similar pulse pumping scheme [33].

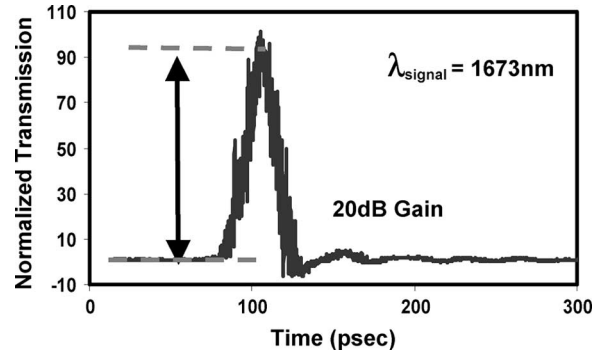


Fig. 10. Time-resolved Raman amplification with signal laser at 1673 nm. A pump on-off gain of 20 dB is obtained. Pump pulse wavelength is 1540 nm.

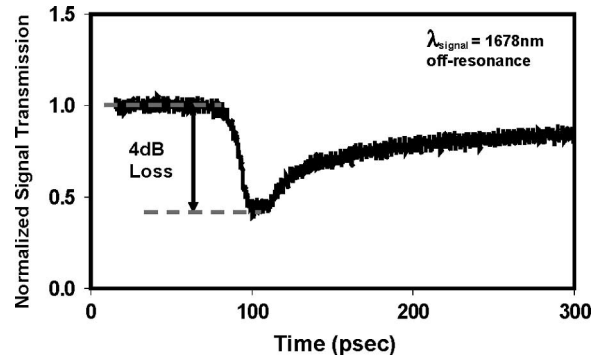


Fig. 11. Time-resolved signal loss with the signal laser at 1678 nm; i.e., outside Raman resonance. Maximum loss of 4 dB and carrier lifetime of 4 ns is obtained.

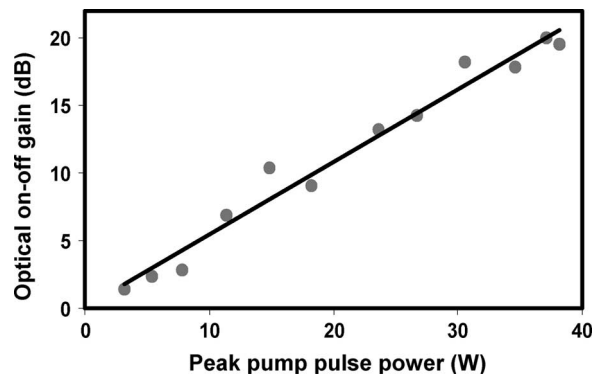


Fig. 12. On-off optical gain as function of peak pump pulse power. Maximum gain of 20 dB is obtained.

The net free carrier loss and the free carrier lifetime can be measured by performing the same measurement with the signal laser tuned away from the Raman peak. This is shown in Fig. 11. Maximum loss due to the combined FCA loss was measured to be 4 dB. Thus, the intrinsic Raman gain in the Silicon waveguide is 24 dB. By extrapolating the exponential decay of the carriers, we estimate a free carrier lifetime of ~ 4 ns. The variation of optical gain as a function of peak pump power coupled into the waveguide is shown in Fig. 12. Optical gain is found to saturate around 37 W of peak pump power. This can be attributed to the pulse breakup and excessive spectral broadening of pump laser in the fiber pigtail preceding the waveguide [33].

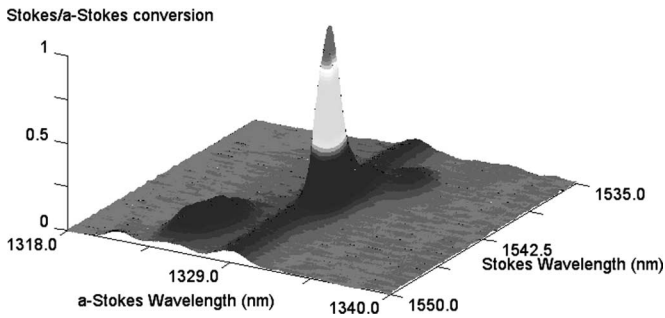


Fig. 13. Measured anti-Stokes spectra versus Stokes signal wavelength. The z-axis represents conversion efficiency, normalized to unity. CW pump laser wavelength is 1428 nm.

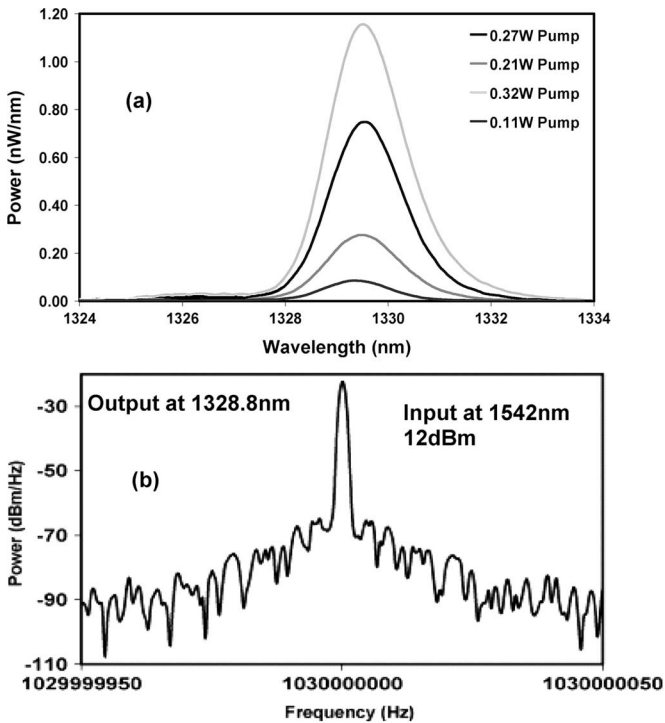


Fig. 14. (a) Anti-Stokes spectrum of converted signal at varying pump powers. (b) RF spectrum of wavelength converted analog data signal at 1.03 GHz. SNR of 47 dB is obtained over 100-Hz bandwidth.

Fig. 13 shows the experimental verification of Raman wavelength conversion in Silicon. The pump laser (at 1427 nm) is coupled to TE mode and the Stokes signal laser is coupled to TE mode. The Stokes signal laser is scanned in a range from 1530 to 1560 nm. Fig. 13 shows the a-Stokes spectra measured as a function of the Stokes signal wavelength. The CW pump power in the waveguide was 0.7 W. There is a clear peak at 1328.8 nm of anti-Stokes emission when the Stokes laser is tuned to Stokes wavelength of 1542.3 nm. The nature of the satellite peaks maybe due to the sinc^2 dependence of the conversion efficiency with phase mismatch.

Fig. 14(a) shows the converted anti-Stokes signal spectrum [39]. The FWHM for wavelength conversion, which is approximately 250 GHz, is determined solely by the pump laser linewidth. The shift in the center wavelength in Fig. 14(a) is due to the slight shift in the local maxima of conversion efficiency

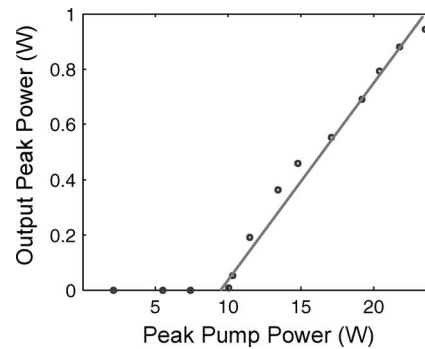


Fig. 15. Measured laser output power with respect to peak pump power. Lasing threshold is measured to be at 9-W peak power level. The slope efficiency obtained by dividing the output peak pulse power by that of the input is $\sim 13\%$.

with increase in pump power. The CARS process is used to perform wavelength conversion from the Stokes to anti-Stokes wavelengths. Fig. 14(b) shows the conversion of 1.03-GHz RF modulation from 1542 to 1328.5 nm [38]. The input RF signal power applied to the Stokes wavelength is shown in the inset. The measured electrical signal to noise ratio (SNR) is 47 dB over 100 Hz. We note that from the application point of view, the 1320- and 1550-nm bands are the two most important bands in optical communication. The measured conversion efficiency was approximately 10^{-5} . As mentioned previously, a number of design approaches are available for phase matching a silicon waveguide and for realizing high conversion efficiency [39].

Fig. 15 shows the measured characteristics for the first silicon Raman laser [4]. The laser, demonstrated in 2004, operated in the pulse mode and consisted of a 1.7-cm-long silicon waveguide gain medium with the experimental setup similar to Fig. 9 and an external cavity form via a fiber loop. The laser has a threshold of 9 W peak pulse power (corresponding to a few milliwatts of average power), and was able to produce output pulses with over 2.5-W peak power at a 25-MHz repetition rate. The demonstration was a major milestone, as it clearly showed that silicon can indeed lase. The strong lasing characteristics and high conversion efficiency ($\sim 13\%$) of the prototype laser showed that silicon Raman lasers must be considered as a practical and compact alternative to fiber Raman lasers.

In 2005, Intel Corporation demonstrated the first CW silicon Raman laser [6]. The device was a 5-cm-long silicon waveguide with a cavity formed by high reflectivity (HR) coating the chip facets. CW operation was achieved by using a reverse bias p-n junction to sweep out the TPA generated free carriers, an approach that was previously proposed in 2004 [22], [23], [29]. Fig. 16 shows the laser input-output behavior at reverse bias voltages of 5 and 25 V. The laser produced a maximum output power of ~ 9 mW at 25-V reverse bias with 600 mW of CW pump power inside the waveguide. The CW operation is an important step in the development of silicon Raman lasers. One drawback of the reverse bias carrier sweepout approach is the electrical power dissipated on the chip. With a reverse current of approximately 50 mA expected for this device, the laser dissipates an on-chip electrical power of more than 1 W. From this perspective, methods that can drastically reduce carrier lifetime, and hence mitigate the need for active carrier removal, are

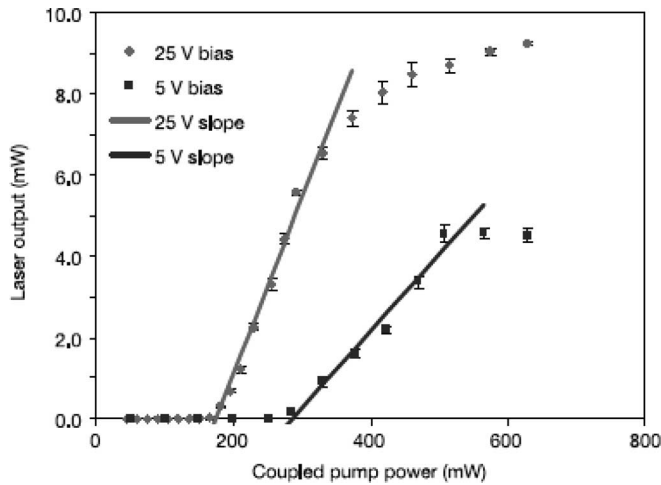


Fig. 16. Threshold characteristics of CW silicon Raman laser demonstrated in a 5-cm silicon waveguide and with using reverse biased p-i-n diode for carrier sweepout [6].

a desired. As a compromise, reduction of the required sweepout voltage will reduce the electrical power dissipation.

The ability to integrate a p-n junction along with the gain medium offers the exciting possibility of intracavity gain switching [5]. This feature was utilized recently to demonstrated electrical modulation using an integrated p-n junction diode. Optical loss in silicon and hence the net optical gain in the laser cavity is proportional to the free carrier density in silicon, with a dependence that is described as $\Delta\alpha = 1.7 \times 10^{-17} \cdot \Delta N$, where $\Delta\alpha$ is the change in loss caused by ΔN change in free carrier density [25], [26]. The linear dependence of free carrier density on diode forward current provides direct electronic modulation of the intracavity gain. The laser will be turned off when the loss induced by diode current exceeds the gain per round trip in the cavity. Hence, the device will function as a “normally on” switch that is turned off when forward bias is applied to the p-n junction diode. The turn-on and turn-off times are dependent of the photon build up in the resonator and the carrier injection time of the diode, respectively. While the modulation speed is limited in this experiment to 1 MHz, the result clearly demonstrates the switching capability of the silicon Raman laser.

This idea, first demonstrated at UCLA, has been extended by Intel in a demonstration of an electrically switched Raman amplifier, with the device representing a loss-less modulator [40].

V. GeSi RAMAN DEVICES

The introduction of germanium in the overall scheme of non-linear Raman processes in silicon offers new avenues for tailoring the device characteristics. In particular are the following [41].

- 1) The strain caused by the difference in the lattice constants of Si and Ge, along with the composition effect, provides mechanisms for tuning the Stokes shift associated with the dominant Si-Si (500 cm^{-1}) vibrational mode [42]. In addition, the presence of Si-Ge modes (400 cm^{-1}) and Ge-Ge modes (300 cm^{-1}) provide flexibility in pump and signal wavelengths.

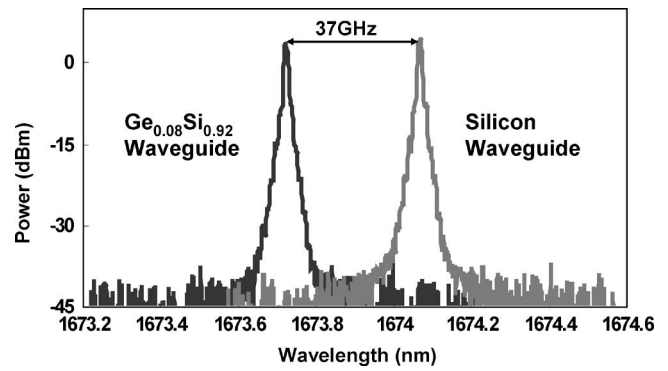


Fig. 17. Stimulated Raman spectra of GeSi waveguides compared to that of silicon waveguide. A 37-GHz red shift in the Stokes wavelength is observed. Pump wavelength was 1539 nm.

- 2) Spectral broadening can be achieved by graded Ge composition.
- 3) The growth of Si_mGe_n superlattices in Silicon can offer the possibility of zone folding of acoustic phonon modes, and hence increase the number of Raman active modes, in the medium.
- 4) When grown on an SOI substrate, the use of double cladding in the vertical direction can improve fiber waveguide coupling efficiency.
- 5) The strain resulting in birefringence [43] can provide an addition degree of freedom for phase matching in the wavelength conversion process. Stress also results in broadening of the gain spectrum via splitting of the degenerate optical phonon modes.
- 6) Higher carrier mobility, and hence diffusion constant, in SiGe reduces the effective lifetime in the waveguide. This reduces the losses associated with the free carriers that are generated by two-photon absorption (TPA). However, this benefit will be countered by the higher TPA coefficient in GeSi.

Recently, the first GeSi optical amplifier and laser was demonstrated [41]. A pulsed gain of 16 dB and lasing with sharp threshold characteristics were observed for $\text{Ge}_{0.08}\text{Si}_{0.92}$ rib waveguides. The Stokes spectrum, shown in Fig. 17, exhibits a 37-GHz red shift which is in qualitative agreement with a model that takes into account the effect of composition and strain on the optical phonon frequency [41]. These results suggest that the spectrum of Raman scattering can be engineered using the GeSi material system. As a result, GeSi Raman devices represent an exciting topic for future research and development.

VI. CONCLUSION

This paper has reviewed recent results on light generation, amplification, and wavelength conversion in silicon and GeSi using stimulated Raman processes. These effects are routinely observed in optical fiber; however, several kilometers of length are required to do so. What has enabled us to achieve these processes on millimeter length scales on a chip are two fundamental differences between an optical fiber and a silicon microstructure.

The first is the difference in atomic structures. Vibrational modes in silica broaden into bands; hence, the Raman gain has a very large bandwidth and a low peak value, requiring long interaction lengths for the effect to be observed. In contrast, silicon is single crystal and supports only three degenerate optical vibration modes. The result is a much narrower gain bandwidth, but a much higher gain peak (nearly 10^3 – 10^4 times higher). Second, consider the difference in modal areas. The large index-contrast in the silicon/SiO₂ waveguides results in a mode area that is approximately 100 times smaller (assuming $0.8 \mu\text{m}^2$ waveguides) than in a standard single mode fiber (mode area = $80 \mu\text{m}^2$). The proportionally higher power density in the silicon waveguide lowers the threshold for nonlinear optical processes.

The intrinsic Raman bandwidth in silicon is 105 GHz, and it is broadened in the experiments by the pump laser linewidth (typically ~ 2 nm). The resulting bandwidth is sufficient for amplifying several WDM channels. The bandwidth can be broadened by broadening the pump linewidth even further (although this reduces the peak gain), or by using multiple pump wavelengths. The Raman phenomenon is fully tunable; the tuning range is only limited by the available pump wavelengths. This is an advantage over the nanocrystal approach for light generation and amplification. In addition, the Raman Effect can also perform wavelength conversion. Another important advantage of this approach is that it does not require rare-earth dopants or nanostructures. Hence, it is truly compatible with silicon IC manufacturing. A limitation of the Raman approach is the fact that it is optically pumped. However, it has been shown that silicon Raman lasers can be electronically switched or modulated using intracavity gain-loss modulation. Therefore, these lasers or similarly amplifiers can be interfaced with on-chip electronic circuitry. Raman amplification and lasing in GeSi waveguides has recently been demonstrated. The GeSi material system provides an opportunity to engineer the, otherwise rigid, Raman spectrum of silicon. Owing to the enhanced carrier mobility, GeSi is being pursued by the CMOS IC industry for future high speed circuits. This provides another impetus for investigating GeSi Raman devices.

Going forward, low loss waveguides with small cross sections are required for realizing high performance devices. Surface roughness produces strong scattering and high propagation loss due to the high index contrast between the silicon waveguide core and the cladding (air or SiO₂). As such, the losses of silicon waveguides tend to increase with reduction in cross section. Fortunately, new waveguide fabrication processes that are in development promise low-loss waveguides with submicron cross sections [44], [45]. Naturally, one must be able to efficiently couple light into these structures. Several novel approaches for high efficiency coupling into submicron waveguides have also been developed [45].

REFERENCES

- [1] M. Paniccia, M. Morse, and M. Salib, "Integrated photonics," in *Silicon Photonics*, L. Pavesi and D. J. Lockwood, Eds. New York: Springer-Verlag, 2004, p. 276.
- [2] Z. Gaburro, "Optical interconnect," in *Silicon Photonics*, L. Pavesi and D. J. Lockwood, Eds. New York: Springer-Verlag, 2004, ch. 4, pp. 121–176.
- [3] B. Jalali, S. Yegnanarayanan, T. Yoon, T. Yoshimoto, I. Rendina, and F. Coppinger, "Advances in silicon-on-insulator optoelectronics," *IEEE J. Sel. Topics Quantum Electron.*, vol. 4, no. 6, pp. 938–947, Nov.–Dec. 1998.
- [4] O. Boyraz and B. Jalali, "Demonstration of a silicon Raman laser," *Opt. Express*, vol. 12, pp. 5269–5273, 2004.
- [5] O. Boyraz and B. Jalali, "Demonstration of directly modulated silicon Raman laser," *Opt. Express*, vol. 13, pp. 796–800, 2005.
- [6] H. Rong, R. Jones, A. Liu, O. Cohen, D. Hak, A. Fang, and M. Pannicia, "A continuous-wave Raman silicon laser," *Nature*, vol. 433, pp. 725–728, 2005.
- [7] R. Claps, D. Dimitropoulos, Y. Han, and B. Jalali, "Observation of Raman emission in silicon waveguides at $1.54 \mu\text{m}$," *Opt. Express*, vol. 10, pp. 1305–1313, 2002.
- [8] R. Claps, D. Dimitropoulos, V. Raghunathan, Y. Han, and B. Jalali, "Observation of stimulated Raman scattering in silicon waveguides," *Opt. Express*, vol. 11, pp. 1731–1739, 2003.
- [9] R. Claps, V. Raghunathan, D. Dimitropoulos, and B. Jalali, "Anti-stokes Raman conversion in silicon waveguides," *Opt. Express*, vol. 11, pp. 2862–2872, 2003.
- [10] A. Yariv, *Quantum Electronics*, 3rd ed. New York: Wiley, 1988.
- [11] P. Y. Yu and M. Cardona, *Fundamentals of Semiconductors*, 3rd ed. New York: Springer-Verlag, 1996.
- [12] P. A. Temple and C. E. Hathaway, "Multiphonon Raman spectrum of silicon," *Phys. Rev. A, Gen. Phys.*, vol. 7, p. 3685, 1973.
- [13] D. Dimitropoulos, B. Houshmand, R. Claps, and B. Jalali, "Coupled-mode theory of Raman effect in silicon-on-insulator waveguides," *Opt. Lett.*, vol. 28, pp. 1954–1956, 2003.
- [14] J. M. Ralston and R. K. Chang, "Spontaneous-Raman-scattering efficiency and stimulated scattering in silicon," *Phys. Rev. B, Condens. Matter*, vol. 2, pp. 1858–1862, 1970.
- [15] J. H. Yee and H. H. M. Chau, "Two-photon indirect transition in GaP crystal," *Opt. Commun.*, vol. 10, pp. 56–58, 1974.
- [16] K. W. DeLong and G. I. Stegeman, "Two-photon absorption as a limitation to all-optical waveguide switching in semiconductors," *Appl. Phys. Lett.*, vol. 57, no. 20, pp. 2063–2064, 1990.
- [17] A. Villeneuve, C. C. Yang, G. I. Stegeman, C. N. Ironside, G. Scelsi, and R. M. Osgood, "Nonlinear absorption in a GaAs waveguide just above half the band gap," *IEEE J. Quantum Electron.*, vol. 30, no. 5, pp. 1172–1175, May 1994.
- [18] A. M. Darwish, E. P. Ippen, H. Q. Lee, J. P. Donnelly, and S. H. Groves, "Optimization of four-wave mixing conversion efficiency in the presence of nonlinear loss," *Appl. Phys. Lett.*, vol. 69, pp. 737–739, 1996.
- [19] Y.-H. Kao, T. J. Xia, and M. N. Islam, "Limitations on ultrafast optical switching in a semiconductor laser amplifier operating at transparency current," *J. Appl. Phys.*, vol. 86, pp. 4740–4747, 1999.
- [20] K. Suto, T. Kimura, T. Saito, and J. Nishizawa, "Raman amplification in GaP-AlxGa_{1-x}P waveguides for light frequency discrimination," *Proc. Inst. Elect. Eng.-Optoelectron.*, vol. 145, no. 2, pp. 105–108, Apr. 1998.
- [21] S. Saito, K. Suto, T. Kimura, and J. I. Nishizawa, "80-ps and 4-ns pulse-pumped gains in a GaP-AlGaP semiconductor Raman amplifier," *IEEE Photon. Technol. Lett.*, vol. 16, no. 2, pp. 395–397, Feb. 2004.
- [22] T. K. Liang and H. K. Tsang, "Role of free carriers from two-photon absorption in Raman amplification in silicon-on-insulator waveguides," *Appl. Phys. Lett.*, vol. 84, no. 15, pp. 2745–2747, 2004.
- [23] R. Claps, V. Raghunathan, D. Dimitropoulos, and B. Jalali, "Influence of nonlinear absorption on Raman amplification in silicon waveguides," *Opt. Express*, vol. 12, pp. 2774–2780, 2004.
- [24] A. R. Cowan, G. W. Rieger, and J. F. Young, "Nonlinear transmission of $1.5 \mu\text{m}$ pulses through single-mode silicon-on-insulator waveguide structures," *Opt. Express*, vol. 12, pp. 1611–1621, 2004.
- [25] R. A. Soref and B. R. Bennett, "Electrooptical effects in silicon," *IEEE J. Quantum Electron.*, vol. QE-23, no. 1, pp. 123–129, Jan. 1987.
- [26] R. J. Bozeat, S. Day, F. Hopper, F. P. Payne, S. W. Roberts, and M. Asghari, "Silicon based waveguides," in *Silicon Photonics*, L. Pavesi and D. J. Lockwood, Eds. New York: Springer-Verlag, 2004, ch. 8, pp. 269–294.
- [27] M. A. Mendicino, "Comparison of properties of available SOI materials," in *Properties of Crystalline Silicon*, R. Hull, Ed. London, U.K.: IEE INSPEC, 1998, pp. 992–1001.
- [28] J. L. Freeouf and S. T. Liu, "Minority carrier lifetime results for SOI wafers," in *Proc. IEEE Int. SOI Conf.*, Tucson, AZ, Oct. 1995, pp. 74–75.
- [29] D. Dimitropoulos, R. Jhaveri, R. Claps, J. C. S. Woo, and B. Jalali, "Lifetime of photogenerated carriers in silicon-on-insulator rib waveguides," *Appl. Phys. Lett.*, vol. 86, p. 071115, 2005.

- [30] R. Espinola, J. Dadap, R. Osgood, S. J. McNab, and Y. A. Vlasov, "Raman amplification in ultrasmall silicon-on-insulator wire waveguides," *Opt. Express*, vol. 12, no. 16, pp. 3713–3718, 2004.
- [31] R. Jones, H. Rong, A. Liu, A. W. Fang, M. J. Paniccia, D. Hak, and O. Cohen, "Net continuous wave optical gain in a low loss silicon-on-insulator waveguide by stimulated Raman scattering," *Opt. Express*, vol. 13, pp. 519–525, 2005.
- [32] E. Golovchenko, P. V. Mamyshev, A. N. Pilipetskii, and E. M. Dianov, "Mutual influence of the parametric effects and stimulated Raman scattering in optical fibers," *IEEE J. Quantum Electron.*, vol. 26, no. 10, pp. 1815–1820, Oct. 1990.
- [33] O. Boyraz and B. Jalali, "Demonstration of 11dB fiber-to-fiber gain in a silicon Raman amplifier," *IEICE Electron. Express*, vol. 1, no. 14, pp. 429–434, 2004.
- [34] T. K. Liang and H. K. T sang, "Efficient Raman amplification in silicon-on-insulator waveguides," *Appl. Phys. Lett.*, vol. 85, pp. 3343–3345, 2004.
- [35] Q. Xu, V. R. Almeida, and M. Lipson, "Time-resolved study of Raman gain in highly confined silicon-on-insulator waveguides," *Opt. Express*, vol. 12, pp. 4437–4442, 2004.
- [36] A. Liu, H. Rong, M. Paniccia, O. Cohen, and D. Hak, "Net optical gain in a low loss silicon-on-insulator waveguide by stimulated Raman scattering," *Opt. Express*, vol. 12, no. 18, pp. 4261–4268, 2004.
- [37] V. Raghunathan, O. Boyraz, and B. Jalali, "20 dB on-off Raman amplification in silicon waveguides," presented at the CLEO 2005, Baltimore, MD, May 2005, Paper CMU1.
- [38] V. Raghunathan, R. Claps, D. Dimitropoulos, and B. Jalali, "Parametric Raman wavelength conversion in scaled silicon waveguides," *IEEE J. Lightw. Technol.*, vol. 23, no. 6, pp. 2094–2012, Jun. 2005.
- [39] D. Dimitropoulos, V. Raghunathan, R. Claps, and B. Jalali, "Phase-matching and nonlinear optical processes in silicon waveguides," *Opt. Express*, vol. 12, p. 2774, 2003.
- [40] R. Jones, A. Liu, H. Rong, M. Paniccia, O. Cohen, and D. Hak, "Lossless optical modulation in a silicon waveguide using stimulated Raman scattering," *Opt. Express*, vol. 13, no. 5, pp. 1716–1723, 2005.
- [41] R. Claps, V. Raghunathan, O. Boyraz, P. Koonath, D. Dimitropoulos, and B. Jalali, "Raman amplification and lasing in SiGe waveguides," *Opt. Express*, vol. 13, pp. 2459–2466, 2005.
- [42] J. C. Tsang, P. M. Mooney, F. Dacol, and J. O. Chou, "Measurements of alloy composition and strain in thin $\text{Ge}_x\text{Si}_{1-x}$ layers," *J. Appl. Phys.*, vol. 75, pp. 8098–8108, 1994.
- [43] D.-X. Xu, P. Cheben, D. Dalacu, A. Delage, S. Janz, B. Lamontagne, M.-J. Picard, and W. N. Ye, "Eliminating the birefringence in silicon-on-insulator ridge waveguides by use of ridge cladding stress," *Opt. Lett.*, vol. 29, no. 20, pp. 2384–2386, 2004.
- [44] P. Koonath, K. Kishima, T. Indukuri, and B. Jalali, "SIMOX sculpting of 3-D nano-optical structures," in *Proc. IEEE/LEOS Annu. Meeting*, Tucson, AZ, 2003, vol. 2, pp. 558–559.
- [45] T. Tsuchizawa, K. Yamada, H. Fukuda, T. Watanabe, J. Takahashi, M. Takahashi, T. Shoji, E. Tamechika, S. Itabashi, and H. Morita, "Microphotonic devices based on silicon microfabrication technology," *IEEE J. Sel. Topics Quantum Electron.*, vol. 11, no. 1, pp. 232–240, Jan.–Feb. 2005.

Bahram Jalali (S'86–M'89–SM'97–F'04) is the Professor of Electrical Engineering, Director of the DARPA Center for Optical A/D Systems Technology (COAST), and Director of the Optoelectronic Circuits and Systems Laboratory at the University of California, Los Angeles (UCLA). From 1988 to 1992, he was a Member of the Technical Staff at the Physics Research Division, AT&T Bell Laboratories, Murray Hill, NJ, where he conducted research on ultrafast electronics and optoelectronics. While on sabbatical leave from UCLA from 1999 to 2001, he founded Cognet Microsystems, a Los Angeles-based fiber-optic component company. He served as the company's CEO, President, and Chair, from the company's inception through its acquisition by Intel Corporation in April 2001. From 2001 to 2004, he served as a Consultant at Intel Corporation. His current research interests are in microwave photonics, integrated optics, and fiber-optic ICs. He has published over 200 scientific papers in international peer-reviewed journals and conferences, and holds six U.S. patents with five patents pending.

Prof. Jalali is a Fellow of OSA and is a Full Member of the California Nano Systems Institute (CNSI). He was chosen by *Scientific American* as one of the 50 Leaders Shaping the Future of Technology, in 2005. His work in demon-

strating the first silicon laser was cited by *MIT Technology Review* as one of the top 10 technology trends. He is a Chair of the Los Angeles Chapter of the IEEE Lasers and Electro-Optics Society. He was the General Chair for MWP 2001, the IEEE International Conference on Microwave Photonics (MWP), and Chair of its Steering Committee from 2001 to 2004. He was the recipient of the BridgeGate 20 Award for his contributions to the Southern California economy, and serves on the Board of Trustees of the California Science Center.



Varun Raghunathan (S'05) received the B.S. degree in electrical and electronics engineering from the Birla Institute of Technology and Science, Pilani, India, in 2002, and the M.S. degree in electrical engineering from the University of California, Los Angeles (UCLA), in 2005, where he is currently working toward the Ph.D. degree in electrical engineering.

His research concentrates on the experimental study of stimulated Raman amplification wavelength conversion using parametric Raman conversion processes, and fabrication issues of silicon photonic structures. His research interests include silicon photonics, nonlinear optics, solid state physics, and quantum electronics.

Mr. Raghunathan was awarded a Fellowship by the California Nanosystems Institute (CNSI) for his Master's studies.



Dimitri Dimitropoulos received the B.S. degree from the National Technical University of Athens, Athens, Greece, in 2000, and the M.S. degree from the University of California, Los Angeles (UCLA), in 2003, both in electrical engineering. He is currently working toward the Ph.D. degree in electrical engineering at UCLA.

His research concentrates on silicon integrated optical devices, particularly silicon Raman lasers, amplifiers, and wavelength converters. His research interests include quantum electronics and photonics; noise in physical systems and information theory; and solid-state and plasma physics.



Özdal Boyraz (M'05) received the B.S. degree from Hacettepe University, Ankara, Turkey, in 1993, and the M.S. and Ph.D. degrees from the University of Michigan, Ann Arbor, in 1997 and 2001, respectively, all in electrical engineering.

From 2001 to 2003, he was an R&D Engineer at Xtera Communications. From 2003 to 2005, he was a Postdoctoral Research Fellow in the Department of Electrical Engineering, University of California, Los Angeles. In August 2005, he joined the Department of Electrical Engineering and Computer Science, University of California, Irvine, as an Assistant Professor. He is the author or coauthor of more than 60 scientific publications and holds three U.S. patents.

Dr. Boyraz is a member of the IEEE Lasers and Electro-Optics Society.